# Detection of time delays and directional interactions based on time series from complex dynamical systems

Huanfei Ma, Siyang Leng, Chenyang Tao, Xiong Ying, Jürgen Kurths, Ying-Cheng Lai, and Wei Lin

Phys. Rev. E **96**, 012221 — Published 25 July 2017

DOI: 10.1103/PhysRevE.96.012221

# Accurate detection of time delays and directional interactions based on time series from complex dynamical systems

Huanfei Ma,[1,2] Siyang Leng,[2,3] Chenyang Tao,[2,3] Xiong Ying,[2,3]
Jürgen Kurths,[4,5] Ying-Cheng Lai,[5,6] and Wei Lin[2,3,*]

[1] *School of Mathematical Sciences, Soochow University, Suzhou 215006, China*
[2] *Centre for Computational Systems Biology of ISTBI, Fudan University, Shanghai 200433, China*
[3] *School of Mathematical Sciences and SCMS, Fudan University, Shanghai 200433, China*
[4] *Potsdam Institute for Climate Impact Research, D-14412 Potsdam, and Department of Physics, Humboldt University of Berlin, D-12489 Berlin, Germany*
[5] *Institute for Complex Systems and Mathematical Biology, University of Aberdeen, Aberdeen AB24 3UE, UK*
[6] *School of Electrical, Computer, and Energy Engineering, Arizona State University, Tempe, Arizona 85287-5706, USA*

Data-based and model-free accurate identification of intrinsic time delays and directional interactions is an extremely challenging problem in complex dynamical systems and their networks reconstruction. A model-free method with new scores is proposed to be generally capable of detecting single, multiple, and distributed time delays. The method is applicable not only to mutually interacting dynamical variables but also to self-interacting variables in a time delayed feedback loop. Validation of the method is carried out using physical, biological and ecological models and real data sets. Especially, applying the method to air pollution data and hospital admission records of cardiovascular diseases in Hong Kong reveals the major air pollutants as a cause of the diseases and, more importantly, it uncovers a hidden time delay (about 30-40 days) in the causal influence that previous studies failed to detect. The proposed method is expected to be universally applicable to ascertaining and quantifying subtle interactions (e.g., causation) in complex systems arising from a broad range of disciplines.

*Introduction.* In the physical world, time delays are intimately related to causation, as signals travel at a finite speed. Successful identification of time delays and causal interactions in complex systems is relevant to significant problems of current interest such as precision medicine [1], effective policy and management recommendations on climate and ecosystems [2, 3], energy optimization in urban systems [4], epidemiology [5], control strategy for gene regulation [6], financial regulations [7], human brain functions [8], and human behaviors in online social systems [9]. Traditional methods based on the Granger causality [10, 11] and transfer entropy [12] have issues such as difficulty with nonlinearity and stringent data requirement. Recently a method based on nonlinear dynamical analysis, the convergent cross mapping (CCM) method, was developed [13, 14] to overcome these difficulties, making it possible to infer causality from relatively short time series. In general, accurate detection of time delays to enable inference of causation is an extremely challenging problem. Quite recently, there was an effort in incorporating a single time delay into the CCM scheme [15]. (A detailed discussion of the related works on ascertaining causation can be found in Appendix A.) The purpose of this work is to propose new scores substituting for the old score in the CCM scheme, which then becomes a general, completely data based framework for accurately identifying time delays, regardless of their forms (e.g., single, multiple, or distributed).

In physical systems, time delays and causation are two manifestations of the same principle: the influence of one event (or subsystem) on another one cannot be instantaneous [16–24]. In the real world, time delays may result from the transmission time, switching speed, memory effect, or other physical effects. A real world example is protein expression regulated by transcription factors, where the regulation process goes through a cascade of transcriptions and translations that take from minutes to hours to exert their influences. For a complex system, there are typically multiple or even distributed time delays. While knowledge about the time delays can be used to infer causation, causal analysis can be useful for identifying time delays as well. For example, if one finds that two subsystems of interest are causally linked with specific time delays, then they are nothing but the intrinsic time delays within the whole system and, the "strength" of causation provides a qualitative assessment of the possible time delays.

There are existing methods for identifying time delays [25–31], but they are mostly based on traditional parameter estimation and synchronization, which indeed require *a priori* knowledge about the complex interactions, the exact forms of vector fields, and even the noise types in the system [25–27, 31]. Other methods include invasive external perturbations [28, 29], self feedback [30], or phase-synchronization-based and model-fitting approaches [31]. Clearly, these methods will be ineffective or even of no help for dealing with the real-world data that are experimentally recorded from sys-

* To whom correspondence should be addressed. E-mail: wlin@fudan.edu.cn

tems whose structures are unclear or completely unknown. From the standpoint of dynamics, when time delays are present, a great difficulty arises. Take the CCM method [13] as an example. The present framework assumes that the time series $y(t)$ and $x(t)$ from subsystems $Y$ and $X$, respectively, are on the same footing through the implicit assumption that the directed influence occurs instantaneously. However, since $Y$ receives inputs from $X$ but with time delays, application of the original CCM method may lead to erroneous results, especially when there are measurement errors or even exponential divergence between the dynamical trajectories in $Y$ and $X$. All these call for the development of a *data-based* and *model-free* framework to accurately determine time delays of arbitrary form.

In this work, based on first-principle considerations, we propose a model-free method involving a class of measures (or scores) with the following general trait: when it is plotted versus an assumed, systematically varying time delay variable, distinct peaks (or a distribution) emerge(s), and their locations correspond to the actual time delays in the system. The score is generally defined in terms of cross map evaluation (CME - to be detailed below) between the targeted dynamical variables (time series). The detailed mathematical quantities used in constructing the CME score can vary, which can be, e.g., covariance, mutual information, or simply phase space distance. We demonstrate universally accurate detection of time delays with simulated time series. Applying the CME score to a specific class of real-world data, e.g., pollution and cardiovascular disease data, reveals a hidden time delay that has escaped previous detection. Accuracy, robustness, and universal applicability are the distinct virtue of our CME method, making it appealing to science and engineering applications that demand precise and reliable assessment of time delays.

*Method-CME Score.* Given a time series $x(t)$, one forms a manifold $M_X \in \mathbb{R}^n$ based on delay coordinate embedding [32, 33]: $\boldsymbol{x}(t) = [x(t), x(t-\delta t), \ldots, x(t-(n-1)\delta t)]$, where $n$ is the embedding dimension and $\delta t$ is a proper time lag (In our work, we all use the delayed mutual information (DMI) [33] to determine $\delta t$ and the false nearest neighbor criteria [33, 34] to determine $n$). The classic embedding theorems [32, 35] guarantee that, for a smooth dynamical system, if $n > 2d$, where $d$ is the fractal dimension of the attractor, the reconstructed $M_X$ is topologically conjugated to the original attractor. For two time series $x(t)$ and $y(t)$ from coupled systems, $X$ and $Y$, respectively, the corresponding manifolds $M_X$ and $M_Y$ can be reconstructed accordingly, and the cross map $\Phi : \boldsymbol{x}(t) \to \boldsymbol{y}(t)$ between $M_X$ and $M_Y$ is one-to-one along the time indices. When $X$ drives/causes $Y$, information of $X$ is infused into $M_Y$, so neighboring points on $M_Y$ are generally mapped to neighboring points on $M_X$ by $\Phi^{-1}$ at the same time indices. However, if $X$ has no influence on $Y$, $M_Y$ contains no information about $X$, so neighboring points on $M_Y$ do not necessarily correspond to neighboring points on $M_X$. A quantitative measure to characterize capacity for $\Phi^{-1}$ to map neighbors on $M_Y$ to neighbors on $M_X$ determines the driving "force" from $X$ to $Y$. This idea of cross map [36, 37] was used to determine the prediction directions [13, 38] and recently generalized from local neighborhood to global prediction [39]. Evaluating the neighborhood mapping capacity of $\Phi^{-1}$ is thus key to detecting possible driving from $X$ to $Y$. In the presence of a time delay $\tau$, the driving is supposed to be from $x(t-\tau)$ to $y(t)$ with a cross map $\Psi : \boldsymbol{x}(t-\tau) \to \boldsymbol{y}(t)$. In this case, we consider $z(t) \equiv x(t-\tau)$ and determine the neighborhood mapping capacity of $\Psi^{-1}$ from $\boldsymbol{y}(t)$ to $\boldsymbol{z}(t)$. These considerations lead to our proposed CME method to detect time delays.

Say we are given time series $x(t)$ and $y(t)$ as well as a set of possible time delays: $\Gamma = \{\tau_1, \tau_2, \ldots, \tau_m\}$. For each candidate time delay $\tau_i$, we let $z(t) = x(t-\tau_i)$ and form the manifolds $M_Y$ and $M_Z$ with $n_y$ and $n_z$ being the respective embedding dimensions. For each point $\boldsymbol{y}(\tilde{t}) \in M_Y$, we find $K$ nearest neighbors $\boldsymbol{y}(t_j)$ $(j = 1, 2, \ldots, K)$, which are mapped to the mutual neighbors $\boldsymbol{z}(t_j) \in M_Z$ $(j = 1, 2, \ldots, K)$ by the cross map. We then estimate $\boldsymbol{z}(\tilde{t})$ by averaging these mutual neighbors through $\hat{\boldsymbol{z}}(\tilde{t})|M_Y = (1/K)\sum_{j=1}^{K} \boldsymbol{z}(t_j)$. Finally, we define the CME score as

$$s(\tau) = (n_z)^{-1}\text{trace}\left\{\Sigma_{\hat{\boldsymbol{z}}}^{-\frac{1}{2}}\text{cov}(\hat{\boldsymbol{z}}, \boldsymbol{z})\Sigma_{\boldsymbol{z}}^{-\frac{1}{2}}\right\}, \qquad (1)$$

where $\tau$ is a trial (or candidate) time delay, the function trace$\{\cdot\}$ represents the summation of all the diagonal elements of the underlying matrix, the diagonal matrix $\Sigma_{\boldsymbol{p}}$ contains the diagonal elements of $\text{cov}(\boldsymbol{p}, \boldsymbol{p})$ for $\boldsymbol{p} = \hat{\boldsymbol{z}}, \boldsymbol{z}$, with the covariance matrix being $\text{cov}(\boldsymbol{p}, \boldsymbol{q}) = \mathbb{E}\left[(\boldsymbol{p} - \mathbb{E}[\boldsymbol{p}])^\top(\boldsymbol{q} - \mathbb{E}[\boldsymbol{q}])\right]$, and $\mathbb{E}[\cdot]$ stands for component-wise average in time. It is straightforward to show $0 \le s \le 1$. The larger the value of $s$, the stronger the driving force from $x(t-\tau_i)$ to $y(t)$. In a plot of $s(\tau)$, if there is a peak at $\tau_k \in \Gamma$, the time delay from $X$ to $Y$ can be identified as $\tau_k$. Since $s$ is designed to measure whether the mutual neighbors $\boldsymbol{z}(t_j)$ are in the neighborhood of $\boldsymbol{z}(\tilde{t})$ in the $\mathbb{R}^{n_z}$ space, criteria other than that based on the covariance matrix can be used.

*Results.* To validate our CME method, we begin with a discrete-time logistic model of two non-identical species:

$$X_{t+1} = X_t(\gamma_x - \gamma_x X_t - K_1 Y_{t-\tau_1}),$$
$$Y_{t+1} = Y_t(\gamma_y - \gamma_y Y_t - K_2 X_{t-\tau_2}),$$

where $\gamma_x = 3.78$, $\gamma_y = 3.77$, $K_1$ and $K_2$ are the coupling parameters, and $\tau_1$ and $\tau_2$ are the intrinsic time delays that we aim to determine from time series. Figure 1 shows the detection results for different combinations of $K_1$, $K_2$, $\tau_1$, and $\tau_2$, which indicates that the method can accurately detect single or double delays for unidirectional (i.e., $K_1 = 0$ or $K_2 = 0$) or bidirectional coupling (i.e., $K_1 \neq 0$ and $K_2 \neq 0$). In order to gain more theoretical insight of our CME method, we give a heuristic illustration on the validity of our method. For simplicity, we set $\tau_1 = 0$ and $\tau_2 = v$ in the above logistic model of

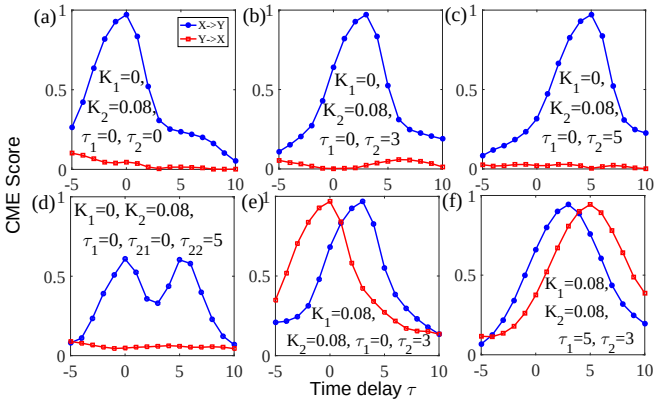


FIG. 1. (Color-online) Accurate detection of time delays and directional interactions in a logistic model of two species. For $n = 2$ and $\delta t = 1$, (a)-(c) single delay under unidirectional coupling. (d) Multiple delays where the coupling term in the population of the second species is $K_2(X_{t-\tau_{21}} + X_{t-\tau_{22}})$. (e)-(f) Multiple delays under bidirectional coupling.

two species. Then, mathematical transformations on the model yield:

$$\begin{aligned} X_{t+1} &= \tfrac{1}{K_2}\left(\gamma_y - \gamma_y Y_{t+v} - \tfrac{Y_{t+1+v}}{Y_{t+v}}\right) \times \\ &\quad \left[\gamma_x - \tfrac{\gamma_x}{K_2}\left(\gamma_y - \gamma_y Y_{t+v} - \tfrac{Y_{t+1+v}}{Y_{t+v}}\right) - K_1 Y_t\right], \\ Y_{t+1} &= \tfrac{1}{K_1}\left(\gamma_x - \gamma_x X_t - \tfrac{X_{t+1}}{X_t}\right) \times \\ &\quad \left[\gamma_y - \tfrac{\gamma_y}{K_1}\left(\gamma_x - \gamma_x X_t - \tfrac{X_{t+1}}{X_t}\right) - K_2 X_{t-v}\right]. \end{aligned} \tag{2}$$

If $K_1 = 0$ and $K_2 \neq 0$, the causal interaction is unidirectional from $X$ to $Y$ with the time delay $v$. In this case, the second equation in Eq. (2) becomes ill-conditioned because $K_1$ appears in a denominator. However, the first equation in Eq. (2) implies that using information about both $Y_{t+1+v}$ and $Y_{t+v}$ gives a more accurate prediction of $X_{t+1}$. In fact, the chaotic attractors of the logistic model have a dimension larger than unity. As a result, our CME score, which takes into account full information about the reconstructed two-dimensional vector, leads to an accurate identification of the delay. If both $K_1$ and $K_2$ are nonzero, the dynamics of $X$ and $Y$ are chaotic and unsynchronized, and the causal interactions between them are bidirectional. In this case, although the term $K_1 Y_t$ appears in the first equation of Eq. (2), it is relatively small by comparing with the terms $\frac{\gamma_x \gamma_y}{K_2} Y_{t+v}$ and $\frac{\gamma_x}{K_2}\frac{Y_{t+1+v}}{Y_{t+v}}$ in this equation, as intuitionally shown in Figs. 2(a)-2(d). Thus, $K_1 Y_t$ can be neglected when predicting $X_{t+1}$, which suggests that it is sufficient to use the information about $Y_{t+1+v}$ and $Y_{t+v}$ to predict $X_{t+1}$. Thus, the proposed CME score enables us not only to ascertain the casual interaction but, more strikingly, to obtain the accurate value of time delay. Analogously as shown in Figs. 2(e)-2(h), the influence of $K_2 X_{t-v}$ in the second equation of Eq. (2) for predicting $Y_{t+1}$ is relatively weak as compared with the terms $\frac{\gamma_y \gamma_x}{K_1} X_t$ and $\frac{\gamma_y}{K_1}\frac{X_{t+1}}{X_t}$. These observations suggest that it is sufficient to use the information about $Y_{t+1+v}$ and $Y_{t+v}$ to predict $X_{t+1}$. Since information about $X_{t+1}$ and $X_t$ is sufficient for predicting $Y_{t+1}$, the CME score indicates instantaneous casual interaction from $Y$ to $X$.

To further test our method for continuous-time systems, a coupled chaotic Lorenz-Rössler (LR) system is considered, which is given by

$$\begin{aligned} &\dot{x}_1 = 10(-x_1 + y_1), \quad \dot{y}_1 = 28x_1 - y_1 - x_1 z_1 + L(y_2), \\ &\dot{z}_1 = x_1 y_1 - (8/3) z_1, \\ &\dot{x}_2 = -\alpha(y_2 + z_2), \quad \dot{y}_2 = \alpha(x_2 + 0.2 y_2) + K(x_1), \\ &\dot{z}_2 = \alpha[0.2 + z_2(x_2 - 5.7)], \end{aligned}$$

where $K(x_1)$ and $L(y_2)$ designate bidirectional couplings between a Lorenz oscillator in the variable $x_1$ and a Rössler system in $y_2$, and $\alpha$ is a scaling factor [40, 41]. For discrete delays, we set $K(x_1) = C x_1(t - \tau_1)$ and $L(y_2) = D y_2(t - \tau_2)$ with parameters $C$ and $D$, the coupling strengths, and $\tau_1 = 3$ and $\tau_2 = 4$, the delays. Let $x_1(t)$ and $y_2(t)$ be the available time series. Figures 3(a)-3(b) show that for most parameter sets, the plots of $s(\tau)$ in both directions exhibit peaks at the true values of the time delays. However, for very weak strengths but larger $\alpha$, as shown in Fig. 3(b), the true delay cannot be detected in the direction from the Rössler oscillator to the Lorenz one. This reveals that our method might not be directly applicable to the case where the coupling signal is very weak. Additionally, as shown in Fig. 3(c), for different distributed time delay as represented by

$$K(x_1) = C \int_{-4}^{-2} k(-\xi) x_1(t + \xi) \mathrm{d}\xi, \quad L(y_2) = 0,$$

the plotted curve of $s(\tau)$ shows different type of plateau on the correct distribution range of the time delay. Here, $k$ is the kennel function which determines the specific distributed type of time delay. Specifically, in Fig. 3(c), the curve $s(\tau)$ shows a horizontal plateau on the interval $[2, 4]$ of the time delay when the kernel function $k$ is set as a uniform distribution; however, the plateau becomes slant when $k$ takes a function of exponential decay. This reveals that our method is practically effective in identifying not only the range of distributed time delays but also their specific distributed types.

There are dynamical systems in which time delays occur through not only mutual couplings but also *self feedback*. To demonstrate the working of our method for such a challenging situation, we consider the Mackey-Glass (MG) system [42] describing the dynamics of blood cell regeneration:

$$\dot{x} = 2x(t - \tau_0) / \left\{1 + [x(t - \tau_0)]^{10} - x\right\},$$

where $\tau_0 \neq 0$ is the time delay, and the time rate of change of $x(t)$ depends on both $x(t)$ and $x(t - \tau_0)$. To apply our method, we select $x(t)$ and $x(t - \tau)$ as the two required time series. Figure 3(d) shows that the plot of $s(\tau)$ exhibits two peaks at $\tau = 0$ and $\tau = \tau_0$, respectively, for larger $\tau_0 = 3$ or 5 which induces chaotic dynamics in

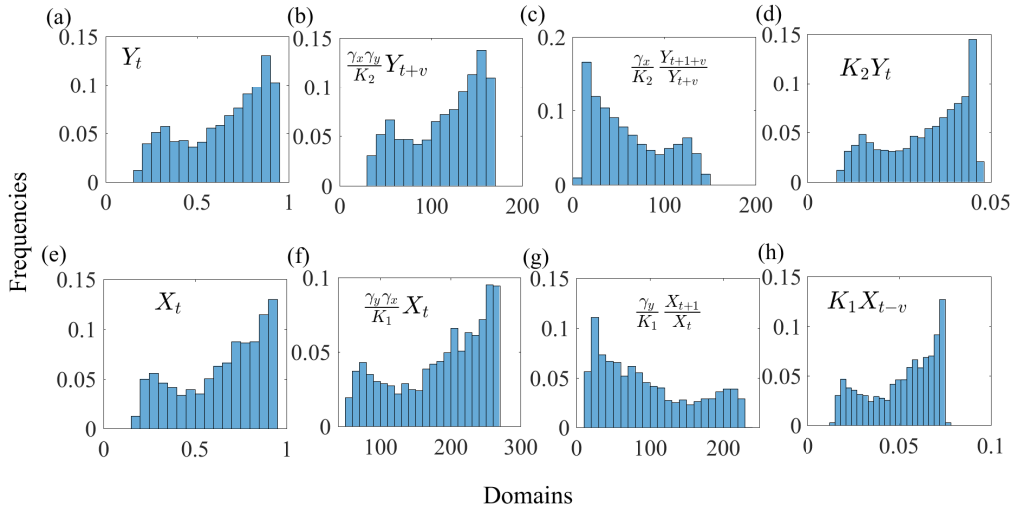


FIG. 2. (Color-online) Distributions of terms in the first equation (a)-(d) and the second equation (e)-(h) of Eq. (2). The horizontal intervals represents the domains of the relevant quantities and the vertical axis represents the frequencies of the values. The parameters are taken as $v = 3$, $K_1 = 0.05$ and $K_2 = 0.08$, and the length of the time series is $10^3$.

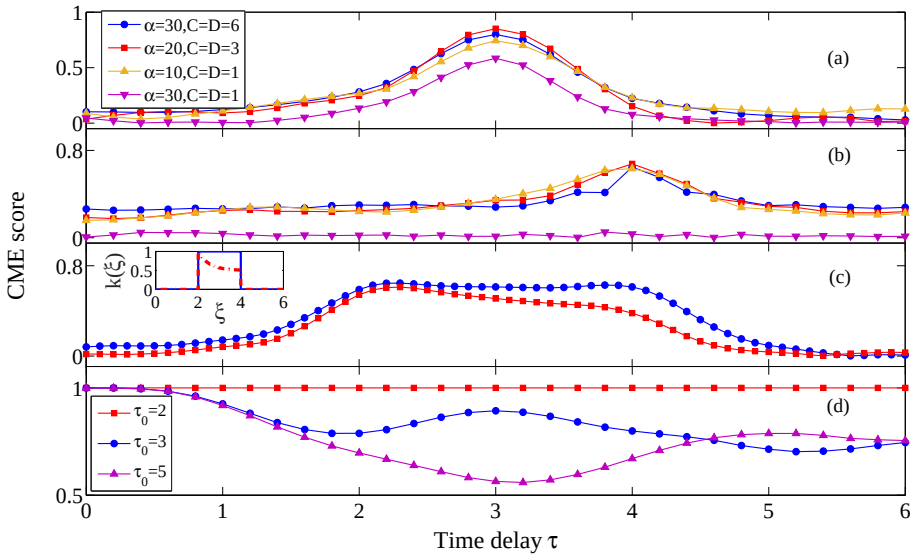


FIG. 3. (Color-online) Identification of diverse types of time delays. For $n = 6$ and $\delta t = 0.12$, identification of discrete time delays in two directions for different parameter sets (a)-(b) and distributed time delay for different kernel function $k$ (c) in different coupled LR systems. (d) For $n = 4$, $\delta t = 0.2$, and different $\tau_0$ inducing different dynamics, successful and failed detections of delays associated with self feedback in the MG system.

the MG system. However, for small $\tau_0$ which only induces periodic dynamics, our method, showing no peak, becomes noneffective because the information in the periodic signal is too few for embedding and delay detection.

More significantly, we apply our method to cope with a dataset of real-world, e.g., air pollution data and hospital admission records of cardiovascular diseases in Hong Kong [43]. The information for the dataset we use here is introduced in Appendix B. Figures 4(a)-4(b) show that there are two pronounced peaks in the CME score from both $NO_2$ and Rspar to Cardio: one at zero while the other at about 30-40 days, where the former reflects the instantaneous effect of air pollution on acute cardiac disease such as heart attack or stroke, which has

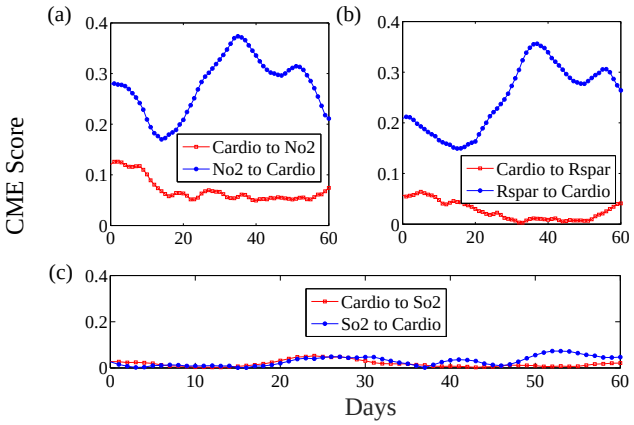


FIG. 4. (Color-online) Identification of time delayed causal influence of air pollutants on cardiac disease from environmental and medical data collected in Hong Kong. The CME scores for disease occurrence against concentrations of pollutants $NO_2$ (a), Rspar (b), and $SO_2$ (c), respectively, are depicted in both directional interactions [i.e., the interaction from disease occurrence to specific pollutant concentration (square lines) and the interaction from pollutant concentration to disease occurrence (dot lines)]. The embedding parameters are $n = 14$ for cardiac disease data, $n = 7$ for the pollutant data, and $\delta t = 1$ day.

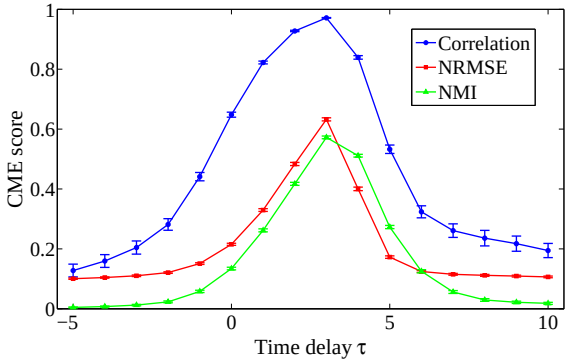


FIG. 5. (Color-online) Performance of alternative CME scores. For the logistic system of two species in Fig. 1 for $K_1 = 0$, $K_2 = 0.08$, $\tau_1 = 0$, and $\tau_2 = 3$, alternative definitions of the CME scores yield the same result of time delay detection as that based on Eq. (1). Shown are the mean value and the corresponding standard deviation for each candidate delay for 100 trails from random initial values.

been widely reported previously [43] and confirmed by statistical analysis [46]. The more pronounced peak at about 30-40 days reflects a delayed effect of causation which, to our knowledge, has not been reported in the literature. (In fact, only the effect of a short term delay within one week was reported [47, 48].) A plausible explanation for the relatively long delay, as uncovered through our method, is that patients with certain chronic diseases such as high blood pressure do not tend to go to hospital until they feel sick, causing the long delay in the disease course from the day they were exposed to air pollution. In addition, sulphur dioxide is also believed to be a causal factor for cardiac disease [46]. However, we find that sulphur dioxide has no significant effect on cardiac disease, as suggested by Fig. 4(c), which is consistent with the result from a recent work [44].

*Remarks.* 1. *Alternative ways to define the CME score.* Our definition of CME score is not limited to the covariance matrix as in Eq. (1). In fact, any appropriately normalized measure of the distance between the predicted and the original points in the $n$-dimensional space would suit. For example, two additional CME scores: one based on normalized mutual information (NMI) [49] and the other exploiting the normalized phase space distance [50], can be used. As shown in Fig. 5 for our example of logistic model of two species, results of time delay identification for these alternatively defined CME scores agree with these based on Eq. (1). Here, the NMI-based score is designed as

$$s = (n_z)^{-1} \sum_{i=1}^{n_z} \left[1 - H\left(\boldsymbol{z}_i|\hat{\boldsymbol{z}}_i\right)/H(\boldsymbol{z}_i)\right],$$

where $H(p)$ is the marginal entropy and $H(p|q)$ is the conditional entropy for two random variables $q$ and $p$. The normalized root-mean-squared error (NRMSE) between vectors $\boldsymbol{p}$ and $\boldsymbol{q}$ is set as

$$\text{NRMSE}(\boldsymbol{p}, \boldsymbol{q}) = \|\boldsymbol{p} - \boldsymbol{q}\| L^{-\frac{1}{2}} \sigma_q^{-1},$$

where $\|\cdot\|$ represents an appropriate vector norm, e.g., the Euclidean norm, $\sigma_q$ is the standard deviation of $\boldsymbol{q}$, and $L$ is the length of vector $\boldsymbol{q}$. In order to scale such distance into a index between 0 and 1, we define an NRMSE-based CME score: $s = \exp(-\xi\theta)$, where $\xi$ is a scaling parameter that can be empirically selected in computation and

$$\theta = (n_z)^{-1} \sum_{i=1}^{n_z} \text{NRMSE}(\boldsymbol{z}_i, \hat{\boldsymbol{z}}_i).$$

We see that $s$ is a normalized score with values in between 0 and 1.

2. *Performance comparison between the CME method and recent methods.* It is noted that some geometric information based methods [15, 52] have also been recently proposed to measure information flow and its delays. To demonstrate the advantage of our CME method over existing methods in a concrete way, we compare its performance with that of a representative method based on CCM [15], through an examination of the effect of increasing the embedding dimension. For the data from the unidirectionally coupled logistic model in Fig. 1, as shown in Fig. 6, our CME method is able to identify the accurate value of the time delay, while the recent

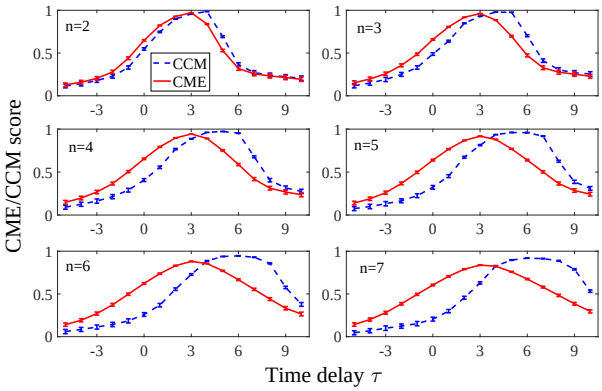


FIG. 6. Performance comparisons of our CME and the recent CCM method with increased embedding dimension. Here, the data is from the unidirectional coupled logistic model with the same parameters as those in Fig. 1 where the true time delay $\tau = 3$. For each intrinsic time delay, the mean value and the corresponding standard deviation are computed based on 100 independent trails.

method [15] fails. In fact, as the embedding dimension $n$ increases (e.g., from 2 to 7), our CME method can consistently detect the true time delay but the method in Ref. [15] fails for all $n > 2$. A plausible explanation is that the method in Ref. [15] is based on CCM measure [13] that uses geometric information about the attractor of the system to detect information flow between variables [38, 39, 51, 52]. As such, the method can infer the existence of casual influences qualitatively but in general cannot yield the accurate values of the time delay. In fact, both the method in Ref. [15] and the error index proposed in Ref. [52] evaluate neighborhood points by using only the first component of the embedding vector, while leaving other components unused. As a result, these methods can only be useful for ascertaining, qualitatively, generalized synchronization and transitive causal chains: they are incapable of identifying the actual values of the time delay. For the method developed in Ref. [52], the estimated time delay lies about the border of the reconstructible domain that needs to be estimated with additional statistical methods, with which identification of distributed time delays is not possible. In contrast, our CME method exploits information about all the components of the reconstructed vector, making it possible to evaluate, in the $n$-dimensional space, the distance between the original point and the predicted point by mutual neighbors, leading to accurate detection of multiple or even distributed time delays.

3. *The requirement on the length of time series.* Since our CME method is based on an extraction of geometric information about the attractor, the length of time series is required to be long enough. Take the time series produced by the above coupled LR system ($\alpha = 30$, $C = 1$ and $D = 0$) for example. When its length is less than $10^3$, the true positive results indicated by the CME scores become unremarkable [see Fig. 7(a)] while the false positive results always arise [see Fig. 7(b)]. As for discrete-time models (or for Poincaré maps induced by continuous-time systems), the admissible length of time series also demands an order of $O(10^3)$ for our CME method. Although, in real-world systems, it is difficult to obtain sufficiently long experimental data, the statistical method of bootstrap [53] can be an option to overcome this difficulty.

4. *The robustness against noise.* In real-world systems, noise is omnipresently observed. Thus, to test the robustness of our CME method against noise, we still use the time series data produced by the coupled Lorenz-Rössler system but deteriorate them by additive white noise with different levels of noise intensity. The levels of noise intensity cover the range of the signal-to-noise ratio (SNR) from $10^2$ to $10^0$. As shown in Figs. 7(c)-7(d), the CME method works robustly and is able to identify the true time delay and directional interaction for the SNR above 5 but the method turns to be failed as the noise intensity becomes strong enough and the SNR becomes weaker.

5. *The influence of coupling strength.* Since the CME method is based on the fact that information of $X$ is infused into $Y$'s dynamics when $X(t-\tau)$ drives/couples with $Y(t)$, the method requires the driving "force"/coupling strength to be sufficiently strong. To illustrate this, we consider two unidirectionally-coupled Lorenz systems:

$$\begin{aligned}
&\dot{x}_1 = 10(x_2 - x_1), \quad \dot{x}_2 = 28x_1 - x_2 - x_1x_3,\\
&\dot{x}_3 = x_1x_2 - (8/3)x_3,\\
&\dot{y}_1 = 10(y_2 - y_1), \quad \dot{y}_2 = 28y_1 - y_2 - y_1y_3 + K(x_2, y_2),\\
&\dot{y}_3 = y_1y_2 - (8/3)y_3,
\end{aligned}$$

where the coupling term $K(x_2, y_2) = C[x_2(t-\tau) - y_2(t)]$, $C$ is the coupling strength, and $\tau = 3$. When the coupling strength $C$ is very small, the driving force from $x_2(t-\tau)$ is extremely weak and thus cannot be detected by the CME method. As $C$ increases, the time delay and interaction detection becomes more and more accurate [see Figs. 7(e)-7(f)]. For $C$ larger than 3, $y_2(t)$ synchronizes with $x_2(t-\tau)$ [see the inset in Fig. 7(f)] and the CME method still works efficiently if the anticipation mode is not taken into consideration.

*Conclusion.* We have developed a completely data-based and model-free method to accurately detect the intrinsic time delays associated with mutual interactions in nonlinear and complex dynamical systems. The main advantage of our method, as compared with previous methods, lies in its universal applicability to all kinds of time delays: single, multiple, self-loop, or even distributed. We validate the method using simulated data from classic nonlinear dynamical systems and real world data. Since time delay and causation are intimately related, we anticipate general suitability of our method for unraveling subtle interactions in complex dynamical systems arising from a broad range of fields in science and engineering.

*Acknowledgement.* W.L. and H.M. were supported by NSFC (Grant Nos. 11322111, 11301366, and

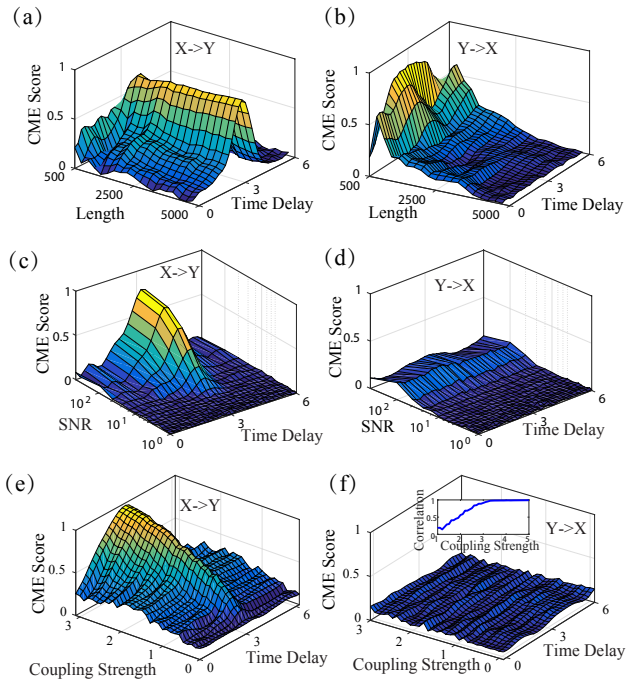


FIG. 7. Performances of the CME method with various factors. (a)-(b): CME scores with the growth of the length of time series produced by a specific coupled LR system. Here, $X$ and $Y$ stand, respectively, for $x_1$ and $y_2$ in the system. (c)-(d): CME scores with the growth of the SNR for the noise-deteriorated time series of the above coupled Lorenz-Rössler system. (e)-(f): CME scores with the growth of the coupling strength for the unidirectionally-coupled Lorenz systems. Here, $X$ and $Y$ stand, respectively, for the driving and the driven systems. The inset in (f) shows the correlation between $x(t-\tau)$ and $y(t)$ as the coupling strength increases.

91530320). Y.C.L. was supported by ARO under Grant No. W911NF-14-1-0504.

[1] F. S. Collins and H. Varmus, New Engl. J. Med. **372**, 793 (2015).
[2] A. M. Neutel, J. A. Heesterbeek JA, and P. C. Ruiter De, Science **296**, 1120 (2002).
[3] E. R. Deyle, et al., Proceedings of the National Academy of Sciences **110** (16), 6430 (2013).
[4] R. Baos R, et al., Renewable and Sustainable Energy Reviews **15**, 1753 (2010).
[5] D. Brockmann and D. Helbing, Science, **342**, 1337 (2013).
[6] J. C. Engelmann, et al. PLoS Comput. Biol. **11**, e1004293 (2015).
[7] N. Joskow and N. Rose, *The Effects of Economic Regulation, in* Handbook of Industrial Organization, vol. **II**, 1449–1506 (ed. by R. Schlamensee and R. Willig R., Amsterdam, Netherlands: North Holland, 1989).
[8] Q. Luo, et al., PLoS Comput. Biol. **9**, e1003265 (2013).
[9] J. Onnela and F. Reedtsochas, Proceedings of the National Academy of Sciences **107** (43),18375 (2010).
[10] N. Wiener, "The Theory of Prediction," (New York, 1956) Chap. 8, pp. 165–183.
[11] C. W. Granger, Econometrica **37**, 424 (1969).
[12] T. Schreiber, Phys. Rev. lett. **85**, 461 (2000).
[13] G. Sugihara, R. May, H. Ye, C.-H. Hsieh, E. Deyle, M. Fogarty, and S. Munch, Science **338**, 496 (2012).
[14] A. A. Tsonis et al., Proceedings of the National Academy of Sciences **112** (11), 3253 (2015).
[15] H. Ye, E. R. Deyle, L. J. Gilarranz, and G. Sugihara, Sci. Rep. **5**, 14750 (2015).
[16] D. S.-I. Niculescu, *Delay Effects on Stability* (Springer, London, 2001).
[17] J.-P. Richard, Automatica **39**, 1667 (2003).
[18] C. M. Marcus and R. M. Westervelt, Phys. Rev. A **39**, 347 (1989).
[19] M. K. S. Yeung and S. H. Strogatz, Phys. Rev. Lett. **82**, 648 (1999).
[20] J. Ruan, L. Li, and W. Lin, Phys. Rev. E **63**, 051906 (2001).
[21] M. Lakshmanan and D. V. Senthilkumar, *Dynamics of Nonlinear Time-Delay Systems* (Springer, Berlin, 2011).
[22] W. Lin, Y. Pu, Y. Guo, and J. Kurths, EPL **102**, 20003 (2013).
[23] G. Kossinets, J. Kleinberg, and D. Watts, in *Proceedings of the 14th ACM SIGKDD International Conference on Knowledge Discovery and Data Mining*, KDD '08 (ACM, New York, NY, USA, 2008) pp. 435–443.
[24] S. Leng, W. Lin, and J. Kurths, Sci. Rep. **6**, 21449 (2016).
[25] J. Tuch, A. Feuer, and Z. J. Palmor, IEEE Trans. Automat. Contr. **39**, 823 (1994).
[26] S. Drakunov, W. Perruquetti, J.-P. Richard, and L. Belkoura, Annu. Rev. Control **30**, 143 (2006).
[27] H. Ma, B. Xu, W. Lin, and J. Feng, Phys. Rev. E **82** (2010).
[28] M. Siefert, Phys. Rev. E **76**, 026215 (2007).
[29] M. D. Prokhorov and V. I. Ponomarenko, Phys. Rev. E **80**, 066206 (2009).
[30] R. Hegger, M. J. Bünner, H. Kantz, and A. Giaquinta, Phys. Rev. Lett. **81**, 558 (1998).
[31] L. Cimponeriu, M. Rosenblum, and A. Pikovsky, Phys. Rev. E **70**, 046213 (2004).
[32] F. Takens, in *Dynamical Systems and Turbulence*, Lecture Notes in Mathematics, Vol. 898, edited by D. Rand and L. S. Young (Springer-Verlag, Berlin, 1981) pp. 366–381.
[33] H. Kantz and T. Schreiber, *Nonlinear Time Series Analysis* (Cambridge University Press, Cambridge, UK, 2004).
[34] M. B. Kennel, R. Brown, and H. D. I. Abarbanel, Phys. Rev. A **45**, 3403 (1992).
[35] T. Sauer, J. A. Yorke, and M. Casdagli, J. Stat. Phys. **65**, 579 (1991).
[36] S. J. Schiff, P. So, T. Chang, R. E. Burke, and T. Sauer, Phy. Rev. E **54**, 6708 (1996).
[37] M. Le Van Quyen, J. Martinerie, C. Adam, and F. J. Varela, Physica D **127**, 250 (1999).
[38] Y. Hirata and K. Aihara, Phy. Rev. E **81**, 016203 (2010).
[39] H. Ma, K. Aihara, and L. Chen, Sci. Rep. **4**, 7464 (2014).
[40] A smaller scaling factor $\alpha$ results in unbounded signals produced by the coupled LR system. However, a larger factor can ensure the production of always bounded dynamics, and even makes the cycle frequencies of the two LR oscillators approach an approximate consensus [41].
[41] P. Laiou and R. G. Andrzejak, Phys. Rev. E **95**, 012210 (2017).
[42] M. Mackey and L. Glass, Science **197**, 287 (1977).
[43] K. Bumseok, Toxico. Res. **30**, 71 (2014).
[44] A. Milojevic, P. Wilkinson, B. Armstrong, K. Bhaskaran, L. Smeeth, and S. Hajat, Heart **100**, 1093 (2014).
[45] T. W. Wong, T. S. Lau, T. S. Yu, A. Neller, S. L. Wong, W. Tam, and S. W. Pang, Occup. Environ. Med. **56**, 679 (1999).
[46] J. Fan and W. Zhang, Ann. Stat. **27**, 1491 (1999).
[47] Y. Xia and W. Härdle, J. Multivar. Ana. **97**, 1162 (2006).
[48] Y. Xia, H. Tong, W. Li, and L.-X. Zhu, J. Roy. Stat. Soc. Ser. B (Stat. Method.) **64**, 363 (2002).
[49] D. Mackay, *Information Theory, Inference, and Learning Algorithms* (Cambridge University Press, Cambridge, UK, 2003).
[50] C. E. Shannon and W. Weaver, *The Mathematical Theory of Communication* (University of Illinois Press, Urbana, IL, 1949).
[51] K. Hlaváčková-Schindler, M. Paluš, M. Vejmelka, and J. Bhattacharya, Phys. Rep. **441**, 1 (2007).
[52] J. Schumacher, T. Wunderle, P. Fries, F. Jäkel, and G. Pipa, Neural Comput. **27**, 1555 (2015).
[53] B. Efron and R. J. Tibshirani, *An Introduction to the Bootstrap* (Chapman & Hall/CRC, London, 1994).
[54] G. Berkeley and C. P. Krauth, *A treatise concerning the principles of human knowledge* (Philadelphia: JB Lippincott & Company, 1874).
[55] J. Geweke, Journal of the American Statistical Association **77**, 304 (1982).
[56] Y. Chen, G. Rangarajan, J. Feng, and M. Ding, Phys. Lett. A **324**, 26 (2004).
[57] N. Ancona, D. Marinazzo, and S. Stramaglia, Phys. Rev. E **70**, 056221 (2004).
[58] Y. Chen, S. L. Bressler, and M. Ding, J. Neurosci. Meth. **150**, 228 (2006).
[59] H. Nalatore, M. Ding, and G. Rangarajan, Phys. Rev. E **75**, 031123 (2007).
[60] D. Marinazzo, M. Pellicoro, and S. Stramaglia, Phys. Rev. Lett. **100**, 144103 (2008).

[61] L. Barnett, A. B. Barrett, and A. K. Seth, Phys. Rev. lett. **103**, 238701 (2009).
[62] J. Sun, C. Cafaro, and E. M. Bollt, Entropy **16**, 3416 (2014).
[63] C. Cafaro, W. M. Lord, J. Sun, and E. M. Bollt, Chaos **25**, 043106 (2015).
[64] J. Sun, D. Taylor, and E. M. Bollt, SIAM J. Dyn. Syst. **14**, 73 (2015).
[65] E. R. Deyle and G. Sugihara, PLoS One **6**, e18295 (2011).
[66] J. C. McBride, *Dynamic Complexity and Causality Analysis of Scalp EEG for Detection of Cognitive Deficits*, Ph.D. thesis, University of Tennessee, Knoxville (2014).
[67] A. Wismüller, X.-X. Wang, A. M. DSouza, and N. B. Nagarajan, arXiv:1407.3809 (2014).
[68] W. Harford, S. Sagarese, M. Nuttall, M. Karnauskas, H. Liu, M. Lauretta, M. Schirripa, and J. Walter, *Can climate explain temporal trends in king mackerel (scomberomorus cavalla) catch-per-unit-effort and landings*, Tech. Rep. (Tech. Rep., SEDAR, SEDAR38-AW-04. SEDAR, North Charleston, SC, 2014).
[69] R. Huffaker and A. Fearne, Proc. Food. Syst, Dyn , 270 (2014).
[70] L. Heskamp, A. S. Meel-van den Abeelen, J. Lagro, and J. A. Claassen, IJCNMH **1(Suppl. 1)**, S20 (2014).

## Appendix A: Brief history of previous relevant works on detecting causality

A common misconception about causation is that it is related to correlation, a simple and symmetric measure but one that does not offer any information about the direction of the causal link. (In fact, three hundred years ago Bishop Berkeley already declared that "correlation does not imply causation" [54].) A classic, well-accepted method is the Granger causality framework originally articulated by Wiener [10] and later formalized by Granger [11] in the setting of multivariate autoregression. The idea behind Granger causality is quite intuitive: for a system consisting of two subsystems, $X$ and $Y$, if $X$ causes $Y$, then the prediction of future $Y$ should be improved by incorporating historical information from $X$. An appealing feature of Granger causality detection is that it can be solved with the method of spectrum decomposition [55]. While it was originally intended for stationary linear systems, the principle of Granger causality can be extended to nonlinear systems but only if they are strongly coupled [56–60]. Methods based on information theory, in particular in terms of mutual information or transfer entropy, were also developed to deal with nonlinear systems [12]. In the special case of Gaussian dynamical variables, the Granger causality and the transfer entropy methods are in fact equivalent to each other [61]. Quite recently, the concept of causation entropy was introduced for causality detection [62–64]. A common difficulty associated with the information-theory based measures lies in the inherently prohibitively large data requirement. For deterministic dynamical systems (or such systems under weak noise), there was a recent breakthrough, the convergent cross mapping (CCM) method [13], as stated in the main text. It is based on the delay-coordinate embedding method [32], a paradigm of nonlinear time series analysis [33, 35, 65]. The main idea is that, a deterministic system, even if it is chaotic, exhibits regularity and short term predictability, which can be exploited for causality detection. In particular, the intrinsic geometrical manifold structure can be reconstructed using the embedding method to yield a topological equivalent of the original system. Suppose we wish to detect and ascertain the causal relation between, say, subsystems $X$ and $Y$. Intuitively, if $X$ causes $Y$, then all the information about $X$ is contained in the manifold of $Y$. Since the manifold of $Y$ can be reconstructed and its short term evolution can be assessed independent of $X$, the state of $X$ can be deduced from that of $Y$, but the converse may not hold. The CCM method can deal with both linear and nonlinear systems with small data sets, and it has been applied to data from different contexts, such as EEG data [66], FMRI [67], fishery data [68], economic data [69], and cerebral auto-regulation data [70].

## Appendix B: Real data sets from environmental monitoring and medicine in Hong Kong

It is generally believed that air pollution is one of the major causes of cardiovascular diseases [43]. To establish this causal relation, we investigate benchmark datasets of air pollutants and disease occurrence in Hong Kong [45, 46]. In particular, daily concentrations (in $\mu$g m$^{-3}$) of nitrogen dioxide ($NO_2$), sulphur dioxide ($SO_2$), and respirable suspended particulate (Rspar) from air monitoring stations in Hong Kong from 1994 to 1997 were collected. Simultaneously recorded was the daily number of cardiovascular diseases admissions into major hospitals in Hong Kong. Figure 8 shows the original data of the daily hospital admissions of cardiovascular disease and the pollutants data in Hong Kong from 1995 to 1997. To avoid the effect of sudden addition of hospital beds in early 1995 [47], we apply the CME method to time series of 1000 days.

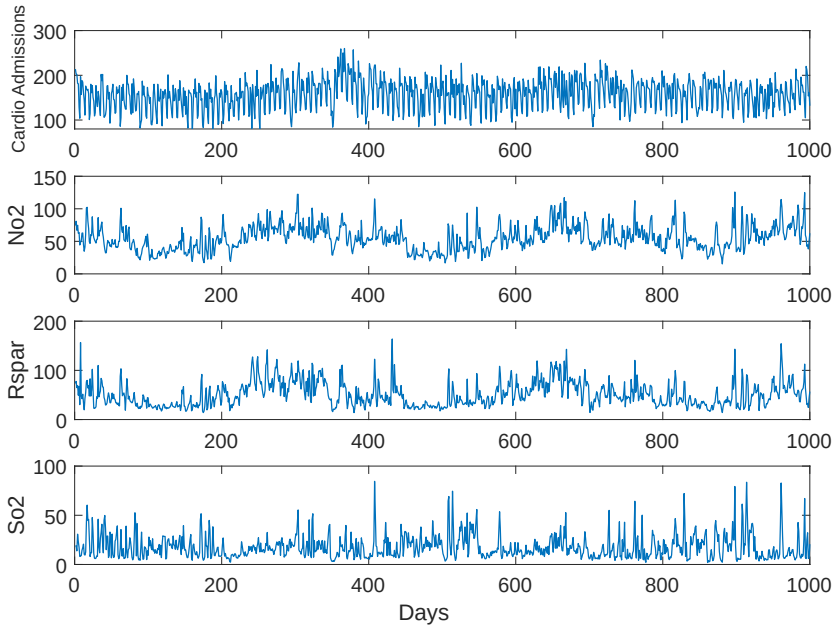


FIG. 8. Original data of the daily hospital admissions of cardiovascular disease and the pollutants data in Hong Kong from 1995 to 1997.